



## ARTICLE

# Anti-PD-L1 mediating tumor-targeted codelivery of liposomal irinotecan/JQ1 for chemo-immunotherapy

Zhi-di He<sup>1,2</sup>, Meng Zhang<sup>1</sup>, Yong-hui Wang<sup>1,2</sup>, Yang He<sup>1,2</sup>, Hai-rui Wang<sup>1,3</sup>, Bin-fan Chen<sup>1,2</sup>, Bin Tu<sup>1,2</sup>, Si-qi Zhu<sup>1,4</sup> and Yong-zhuo Huang<sup>1,2,5,6</sup>

Immune checkpoint blockade therapy has become a first-line treatment in various cancers. But there are only a small percent of colorectal patients responding to PD-1/PD-L1 blockade immunotherapy. How to increase their treatment efficacy is an urgent and clinically unmet need. It is acknowledged that immunogenic cell death (ICD) induced by some specific chemotherapy can enhance antitumor immunity. Chemo-based combination therapy can yield improved outcomes by activating the immune system to eliminate the tumor, compared with monotherapy. Here, we develop a PD-L1-targeting immune liposome (P-Lipo) for co-delivering irinotecan (IRI) and JQ1, and this system can successfully elicit antitumor immunity in colorectal cancer through inducing ICD by IRI and interfering in the immunosuppressive PD-1/PD-L1 pathway by JQ1. P-Lipo increases intratumoral drug accumulation and promotes DC maturation, and thereby facilitates adaptive immune responses against tumor growth. The remodeling tumor immune microenvironment was reflected by the increased amount of CD8<sup>+</sup> T cells and the release of IFN- $\gamma$ , and the reduced CD4<sup>+</sup>Foxp3<sup>+</sup> regulatory T cells (Tregs). Collectively, the P-Lipo codelivery system provides a chemo-immunotherapy strategy that can effectively remodel the tumor immune microenvironment and activate the host immune system and arrest tumor growth.

**Keywords:** tumor-targeted delivery; immunogenic cell death; PD-1/PD-L1 blockade; tumor immune microenvironment; irinotecan; JQ1; immune checkpoint

*Acta Pharmacologica Sinica* (2021) 42:1516–1523; <https://doi.org/10.1038/s41401-020-00570-8>

## INTRODUCTION

The programmed cell death (PD) pathway induces an immunosuppressive state that inhibits T-cell activation and facilitates the tumors to escape immunosurveillance [1]. PD-pathway blockade has become the most important target of cancer immunotherapy, and the PD-1/PD-L1 immune checkpoint inhibitors have attained groundbreaking advances in a broad spectrum of human malignancies, such as melanoma, renal cell carcinoma, and non-small cell lung cancer with microsatellite instability-high (MSI-H) or mismatch repair deficiency (dMMR) [2, 3]. Yet, the low response rate still remains the primary challenge. For example, only 5% of colorectal cancer patients have dMMR or MSI-H [4], and the majority of patients do not benefit from immunotherapy.

In combination with conventional therapy (e.g., chemotherapeutics and radiotherapeutics), the response rate of immune checkpoint therapy could be improved through modulating tumor immune microenvironment (TIME) [5, 6]. Interestingly, some chemotherapeutics may augment the tumor immunogenicity via immunogenic cell death (ICD) of tumor cells and reduce immunosuppression [7]. ICD can promote the release of tumor antigens that sensitize the antigen-presenting cells (i.e., dendritic cells (DCs) and macrophages) in the tumor microenvironment

(TIME). Indeed, anti-PD therapy plus chemotherapy in clinical studies showed improved survival [8].

Irinotecan (IRI), a derivative of camptothecin, is a first-line chemo drug in colorectal cancer, which can inhibit the DNA strand relication via acting on topoisomerase I-DNA complex and thereby induce double-strand DNA breakage and cell death [9]. IRI can induce ICD, upregulate tumor-specific antigens [10, 11], or increase the danger-associated molecular patterns [12].

JQ1 is a small molecule inhibitor of the bromodomain and extraterminal (BET) proteins that regulate the expression of critical oncogenes in a variety of cancers. In specific, JQ1 can intensify the DNA damage responses by lifting the BET protein-mediated inhibition of DNA damage [13]. Of note, JQ1 has been widely used as a small-molecular PD-L1 suppressor to activate anticancer immunity [14, 15].

It was expected that JQ1 could yield a synergistic effect with IRI to augment DNA damage to elicit apoptosis, as well as trigger antitumor immune responses via ICD effect and PD-L1 down-regulation. Therefore, we proposed a liposomal codelivery system for IRI/JQ1 combination therapy. This system was characterized by anti-PD-L1 modification for targeting the PD-L1 overexpressing cancer cells. IRI plays a dual role of chemotherapy and ICD induction. Its DNA damage and antitumor immune responses

<sup>1</sup>State Key Laboratory of Drug Research, Shanghai Institute of Materia Medica, Chinese Academy of Sciences, Shanghai 201203, China; <sup>2</sup>University of Chinese Academy of Sciences, Beijing 100049, China; <sup>3</sup>Artemisinin Research Center, Guangzhou University of Chinese Medicine, Guangzhou 510450, China; <sup>4</sup>Department of Pharmacology, Zhejiang University City College, Hangzhou 310015, China; <sup>5</sup>NMPA Key Laboratory for Quality Research and Evaluation of Pharmaceutical Excipients, Shanghai 201203, China and <sup>6</sup>Zhongshan Branch, the Institute of Drug Research and Development, Chinese Academy of Sciences, Zhongshan 528451, China  
Correspondence: Yong-zhuo Huang (yzhuang@simm.ac.cn)

Received: 14 September 2020 Accepted: 1 November 2020

Published online: 11 December 2020

would be boosted by JQ1 that can reduce the DNA repair and downregulate PD-L1.

## MATERIALS AND METHODS

### Materials

Irinotecan hydrochloride (IRI) and coumarin 6 were purchased from Meilun Company (Dalian, China). JQ1 was purchased from Selleck (Houston, USA). Lecithin (PC), cholesterol, DSPE-PEG<sub>2000</sub>, and DSPE-PEG<sub>2000</sub>-NHS were supplied by AVT Pharmaceutical Co. Ltd (Shanghai, China). RPMI-1640 culture medium, Dulbecco's Modified Eagle's Medium (DMEM) cell culture medium, fetal bovine serum (FBS), and 0.25% trypsin-EDTA were purchased from ThermoFisher (Gibco, Waltham, USA). Recombinant murine granulocyte macrophage colony-stimulating factor (GM-CSF) was obtained from Novus Biologicals (Centennial, USA). Murine interleukin (IL)-4 was purchased from Peprotech (Rocky Hill, USA). Anti-mouse PD-L1 was purchased from Bio X Cell (Lebanon, USA). The primary antibodies of GAPDH and  $\beta$ -actin were from Sigma-Aldrich (St. Louis, USA). The microBCA protein assay kit was from Beyotime Institute of Biotechnology (Haimen, China). The Mouse Lymphocyte separation medium was purchased from Tianjin Haoyang biology Technology (Tianjin, China). Anti-TNF- $\alpha$  (tumor necrosis factor- $\alpha$ ) and anti-CRT antibodies were from Abcam (Cambridge, UK). Fixation/permeabilization solution kit, anti-CD11c, anti-CD80, anti-CD86, anti-CD3, anti-CD4, and anti-CD8 antibodies were purchased from BD Biosciences (Oxford, UK). Foxp3 buffer set, anti-IFN- $\gamma$ , and anti-Foxp3 antibodies were purchased from BioLegend (San Diego, USA). Anti-CD8  $\alpha$  antibody was obtained from Novus Biologicals (Centennial, USA). Anti-IFN- $\gamma$  antibody was from Absin Bioscience Inc. (Shanghai, China). Anti- $\gamma$ H2AX antibody was from ABclonal Technology (Wuhan, China). Anti-caspase 3 was purchased from Cell Signaling Technology (Boston, USA). Mouse IFN- $\gamma$  ELISA Kit was purchased from Dakewe Biotech (Shanghai, China). Mouse HMGB1 ELISA Kit was purchased from Huzhen Biotech (Shanghai, China) and ATP assay kit was from Promega (Madison, USA). DiR (1,1-dioctadecyl-3,3,3-tetramethylindotricarbocyanine iodide) was purchased AmyJet Scientific (Wuhan, China). The horseradish peroxidase (HRP)-conjugated goat anti-rabbit/mouse IgG secondary antibody was purchased from Beyotime (Shanghai, China). The qPCR SYBR<sup>®</sup> Green Master Mix, cDNA synthesis SuperMix kit, and TRleasy<sup>™</sup> Total RNA Extraction Reagent were from Yeasen Biotech Co., Ltd (Shanghai, China). Primers of TNF- $\alpha$  for qPCR were synthesized by Generay Biotech Co., Ltd (Shanghai, China). All other reagents (analytical grade) were purchased from Sinopharm Chemical Reagent (Shanghai, China).

### Cell lines

Murine colon cancer cell line CT26 was obtained from Shanghai Cell Bank of Chinese Academy of Sciences (Shanghai, China). The cells were cultured in RPMI-1640 medium with 10% FBS and 1% penicillin-streptomycin at a humidified 5% CO<sub>2</sub> incubator at 37 °C.

### Animals

Balb/c mice (female, 4–5 weeks) were supplied by Shanghai Laboratory Animal Center (SLAC) Co., Ltd (Shanghai, China), and housed at a standard SPF facility. All the animal experimental procedures were approved by the Institutional Animal Care and Use Committee, Shanghai Institute of Materia Medica, Chinese Academy of Sciences.

### Preparation of IRI hydrochloride-phospholipid complex (IRI-PC)

The IRI-PC complex was prepared by a solvent evaporation method. Briefly, IRI and PC (1:5, w/w) were dissolved in 20 mL chloroform and the solution was agitated at 45 °C for 1.5 h. The organic solvent was subsequently removed by rotary evaporation in a vacuum, yielding a thin film on the wall of the flask. The IRI-PC complex was thus used for liposome preparation.

### Preparation of P-Lipo

The P-Lipo was prepared via a thin film-hydration method. Briefly, the IRI-PC complex was formed as abovementioned and subsequently mixed with 5 mL of chloroform containing lecithin, cholesterol, DSPE-PEG<sub>2000</sub>, and DSPE-PEG<sub>2000</sub>-NHS (20/2/1/0.05, w/w/w/w), and the drug ratio of IRI and JQ1 was 1.7/0.9 (w/w). The chloroform solution was then subjected to rotary evaporation to form a thin film in a round flask. The thin film was hydrated by 5% glucose solution, followed by ultrasonic treatment in water bath. The thus-formed liposomes were extruded through 400- and 200-nm polycarbonate membranes using Avanti Mini-Extruder (Avanti Polar Lipids, Alabaster, USA). The un-encapsulated drugs were removed using a Sephadex G-50 column (GE Healthcare, USA). The P-Lipo was formed by adding anti-PD-L1 antibody (BE0101, Biocell) to the liposomes (anti-PD-L1/DSPE-PEG<sub>2000</sub>-NHS = 1/100, mol/mol) with reaction for 12 h. The size distribution of liposomes was determined by a dynamic light scattering technique (Nano ZS 90, Malvern, UK).

### Characterization of the P-Lipo

The drug encapsulation efficiency and drug-loading capacity were measured using an HPLC system (Agilent 1200, USA) equipped with a C<sub>18</sub> column (5  $\mu$ m, 4.6  $\times$  250 mm, Agilent, USA) with a column temperature of 45 °C. Mobile phase was composed of water and acetonitrile (25/75, v/v) containing 0.01% trimethylamine at a flow rate of 1 mL/min. The detection wavelength was 254 nm. The calculation was as follows:

Drug encapsulation efficiency (%) = mass of encapsulated drug/mass of drug added  $\times$  100%

Drug-loading capacity (%) = mass of encapsulated drug/mass of liposomes  $\times$  100%

The storage stability of P-Lipo was investigated at 4 °C and the particle size of P-Lipo was determined in 1 week. The in vitro cumulative drug release of P-Lipo was measured using a dialysis method, by which PBS (pH 7.4) containing 1% SDS was used as a release medium. The P-Lipo suspension was placed into the dialysis tubes (MWCO 10–12 kDa) in the release medium and shaken at 150 rpm at 37 °C. The drug concentration in the release medium was quantified.

CRT expression and HMGB1 and ATP release in the tumor cells CT26 cells ( $1 \times 10^5$  cells/well) were seeded in the six-well plates overnight. The cells were then treated with IRI at the indicated concentrations for 12 h. The cells were washed using cold PBS and then sequentially stained with a primary rabbit anti-CRT antibody (ab196159, Abcam) for 30 min at 4 °C, and then stained with propidium iodide (50  $\mu$ g/mL) for flow cytometric assay (FACS, BD, USA) to assess CRT expression. The data were expressed as fold-increase calculated by mean fluorescence intensity compared to the PBS control. HMGB1 expression was also determined in the CT26 cells that were seeded on a live cell imaging glass-bottom dish at a density of  $1 \times 10^4$  cells/well overnight. After incubation with 10  $\mu$ M IRI for 12 h, the cells were washed three times and fixed, and then stained with Alexa Fluor<sup>®</sup> 488-conjugated anti-HMGB1 antibody (ab195010, Abcam) for 30 min and with DAPI. The cells were examined by a confocal laser scanning microscope (CLSM, TCS-SP8, Leica, Germany). Extracellular secretion of ATP and HMGB1 was measured using an ATP assay kit and an HMGB1 ELISA assay kit, respectively, according to the manufacturers' instructions. Briefly, CT26 cells were seeded in the 12-well plate at a density of  $1 \times 10^5$  cells/well overnight and then treated with 10  $\mu$ M IRI. After treatment, supernatants were collected for ATP and HMGB1 detection.

### DNA damage assays

For immunofluorescence staining of  $\gamma$ H2AX DNA damage foci, the CT26 cells were seeded on a live cell imaging glass-bottom dish with a density of  $2 \times 10^4$  cells/well overnight and then treated with

1  $\mu\text{M}$  JQ1, 10  $\mu\text{M}$  IRI, or the combo JQ1/IRI for 24 h. The cells were then washed three times with PBS and fixed using 4% paraformaldehyde for 20 min. The cells were blocked with goat serum in Triton X-100 and PBS for 1 h and then incubated with  $\gamma\text{H2AX}$  antibody (AP0099, Abclonal) at 4 °C for 1 h, followed by co-staining with the Alexa647-conjugated secondary antibody for 30 min and with DAPI for CLSM imaging.

**Cellular uptake and tumor penetration of the P-Lipo in vitro**  
To examine the cellular uptake of the liposomes, the CT26 cells were seeded in the 12-well plates at a density of  $2 \times 10^4$  cells/well overnight and then treated with the coumarin 6-labeled liposomes. After 2-h incubation, the cells were stained with DAPI for fluorescent imaging (CARL ZEISS, Germany). The quantitative analysis of the cellular fluorescence intensity was examined by using flow cytometric measurement. In parallel, in a control group, the CT26 cells were pretreated with anti-PD-L1 antibody for 4 h before treatment with the P-Lipo to investigate the competitive blockage.

#### ICD-induced DC maturation

The bone marrow-derived dendritic cells (BMDCs) were obtained following a standard protocol. In brief, the bone marrow monocytes from the femurs and tibias of Balb/c mice (4–6 weeks old) were collected using a standard procedure, and were cultured in DMEM medium containing GM-CSF (20 ng/mL) and IL-4 (10 ng/mL). The culture medium was entirely discarded at day 3 and replaced by a fresh medium as described above. On day 7, the non-adherent cells in the culture supernatant and loosely adherent proliferating DC aggregates were harvested for further experiments. BMDCs were incubated for 24 h with the drug-pretreated tumor cells in which ICD was induced, and the percentage of the mature DCs ( $\text{CD80}^+\text{CD86}^+$ ) was examined using flow cytometry.

#### T-cell activation by the primed DCs

The responder T cells isolated from the spleens of the Balb/c mice were cocultured with the primed BMDCs that were prepared as above at a ratio of 5:1 (T/DC) for 5 days in the complete RPMI-DMEM medium. The IFN- $\gamma$  level in the supernatants was measured using an ELISA kit according to the manufacturer's instructions.

#### In vivo distribution

The CT26 cells ( $5 \times 10^5$ ) were subcutaneously injected into the back of the Balb/c mice to develop a xenograft tumor model. The DiR-labeled liposomes were injected to the mice via tail vein, and the in vivo imaging study was conducted using an IVIS imaging system (Caliper Life Science, Waltham, USA). After 24 h, the mice were sacrificed and the organs were collected for ex vivo imaging.

#### In vivo antitumor efficacy

The CT26 tumor-bearing mice were randomly divided into six groups (six mice per group) and intravenously treated with PBS, IRI, JQ1, IRI-JQ1, Lipo, and P-Lipo at a dose of 45 mg/kg IRI and 15 mg/kg JQ1. When the tumor volume reached around 50  $\text{mm}^3$ , the drugs were given via tail vein injection once every 2 days. The tumor volume was calculated by this formula:

$$\text{Tumor volume (mm}^3\text{)} = \text{length} \times \text{width}^2/2$$

#### Mechanism studies

To elucidate the mechanisms underlying the superior antitumor efficacy of P-Lipo, the CT26-tumor-bearing Balb/c mice were treated by the same procedure as described above and the tumor tissues were then harvested 1-day post the third treatment. The P-Lipo-induced ICD was examined using immunofluorescence staining of CRT. The draining lymph nodes (LNs) and spleens were collected for flow cytometric analysis of the mature DCs and  $\text{CD8}^+$  T cells. The concentration of IFN- $\gamma$  in the serum and tumor was

examined by an ELISA kit. The intratumoral infiltration of Tregs ( $\text{CD4}^+\text{Foxp3}^+$  T cells) and cytotoxic IFN- $\gamma^+\text{CD8}^+$  T cells was evaluated by flow cytometry. PD-L1 expression in the tumor was also examined through flow cytometry. The immunohistochemical examination of the tissue sections was carried out by staining with anti-cleaved caspase 3. The tissue slices were imaged using a confocal laser scanning microscope. The expression of the TNF- $\alpha$  in the CT26 tumor tissues after treatment was also detected using a standard procedure of Western blotting. In addition, the mRNA expression of TNF- $\alpha$  was measured by real-time quantitative polymerase chain reaction (qPCR). Total RNA was isolated with the TRIeasy™ Total RNA Extraction Reagent according to the manufacturer's instructions. Then, cDNAs were amplified using SYBR Green PCR Master Mix with primers (forward: 5'-CGTCAGCCG ATTTGCTATCT-3', reverse: 5'-CGTCAGCCGATTTGCTATCT-3') at a final volume of 20  $\mu\text{L}$ , and the samples were performed in triplicate by the CFX384 Touch Detecting System (Bio-Red, USA). The mRNA expression was normalized with GAPDH mRNA content.

#### Statistical methods

All data are mean  $\pm$  SEM. The bar graphs show the results from three independent experiments. Statistical analysis was calculated by unpaired *t*-test and the therapeutic efficiency in animal study was analyzed using one-way ANOVA. Statistical significance was set at the value of  $P < 0.05$ . Multiple asterisks represent the statistical significance as \* $P < 0.05$ , \*\* $P < 0.01$ , \*\*\* $P < 0.001$ , and \*\*\*\* $P < 0.0001$ .

## RESULTS AND DISCUSSION

### Anticancer synergistic effect of IRI and JQ1 therapy

ICD is characterized by the exposure of calreticulin (CRT) on the cancer cell surface and the release of ATP and HMGB1 during apoptosis [16]. The ICD induction of IRI was investigated and the results showed that exposure of CRT on the IRI-treated CT26 cells was increased, with a dose-dependent pattern (Fig. 1a). The exposed CRT on the cancer cell surface serves as an "eat-me" signal to the antigen-presenting cells (e.g., DCs and macrophages) and elicits antitumor immune responses. IRI also induced a significant extracellular release of HMGB1 (Fig. 1b, c) and ATP (Fig. S1).

To explore the combination therapy of IRI and JQ1, the  $\gamma\text{H2AX}$  DNA foci formation, as an indicator of DNA damage [17], was monitored after treatment. The results showed that the DNA damage foci in the CT26 cells were increased by the co-application with IRI and JQ1 compared to the single treatments (Fig. 1d). Importantly, the ICD effect was much stronger in the combined treatment, reflected by a 50% increase in the exposure of CRT compared to the IRI treatment group (Fig. 1e). Those results revealed that the combination of IRI and JQ1 enhanced the DNA damage and ICD effects. JQ1 has been often used as a small-molecular suppressor of PD-L1 for triggering anticancer immunity, because PD-L1 is a downstream effector of a BET protein-BRD4 [15]. Remarkable PD-L1 downregulation was observed in the CT26 cells treated with JQ1 (Fig. 1f).

### Preparation and characterization of anti-PD-L1 modified liposomes with co-encapsulation of IRI and JQ1

A PD-L1-targeting immunoliposome co-encapsulating IRI and JQ1 (termed P-Lipo) was prepared via a thin film-hydration method. The P-Lipo was about 160 nm with uniform size distribution and exhibited good serum stability and a sustained release pattern (Fig. 2a, b, S2). The encapsulation efficiency was 71.7% for IRI and 45.8% for JQ1 in the P-Lipo.

The successful conjugation of anti-PD-L1 antibody with the non-targeting liposomes (termed Lipo) was confirmed by SDS-PAGE electrophoresis, demonstrated by the upper shift of the band due

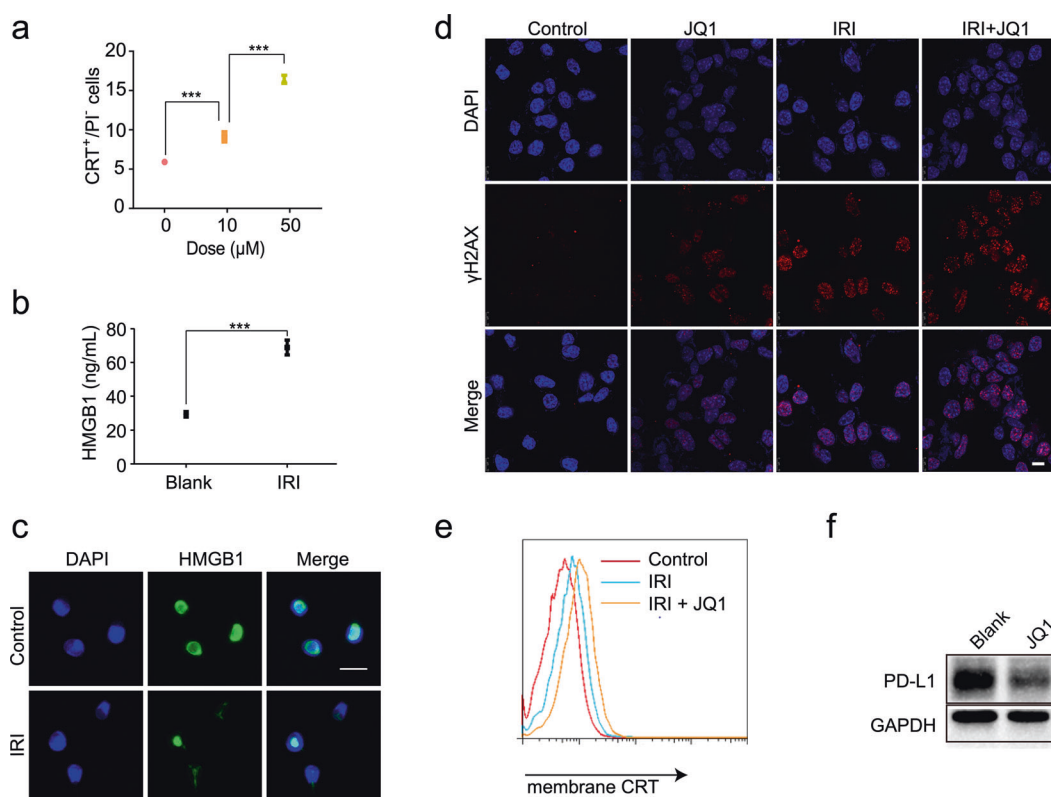


**Fig. 1** ICD effect induced by IRI and synergistic effect of IRI/JQ1 in CT26 cancer cells. **a** IRI-induced CRT exposure. ELISA analysis (**b**) and CSLM examination (**c**) of HMGB1 release of CT26 cells induced by IRI (Scale bar 20  $\mu\text{m}$ ); HMGB1 that is normally located at the nucleus was released from the nucleus during immunogenic cell death, thus causing the diminished fluorescence signal in the nucleus. **d** Representative immunofluorescence images of  $\gamma\text{H2AX}$  DNA damage foci in CT26 cells treated with JQ1 and/or IRI (scale bar 50  $\mu\text{m}$ ). **e** IRI/JQ1 treatment increased CRT exposure. **f** PD-L1 expression in CT26 cells reduced by JQ1 treatment. Mean  $\pm$  SEM. \*\*\* $P < 0.001$ .

to the change in molecular weight (Fig. 2c). Protein smears observed in the lane of P-Lipo was probably due to the lipid content in the samples, which decreased the electrophoretic mobility of antibody chains [18]. The P-Lipo displayed a significantly increased uptake efficiency in the CT26 cells, 1.5-fold higher than the Lipo (Fig. 2d, e). It was attributed to the overexpressed PD-L1 in the CT26 cancer cells (Fig. S3), which thus promoted PD-L1-mediated intracellular delivery.

#### The immune activity of P-Lipo

DCs play key roles in eliciting and regulating the innate and adaptive immune response, which can thus yield a synergistic action with the ICD effect [19, 20]. The ability of P-Lipo to induce immunogenicity of the tumor cells with “danger signals” and promote DC maturation was investigated [21, 22]. The P-Lipo-pretreated tumor cells significantly promoted the maturation of DCs ( $\text{CD11c}^+\text{CD80}^+\text{CD86}^+$ ) (Fig. 2f). Furthermore, these thus-obtained matured DCs were able to stimulate the IFN- $\gamma$  secretion from the autologous T cells; the IFN- $\gamma$  level was higher in the P-Lipo than other groups (Fig. 2g). Those results suggested that the P-Lipo efficiently induced the ICD effect in the CT26 cells that subsequently promoted the antigen presentation by DCs and thus activated T-cell immunity.

**In vivo studies of tumor-targeting delivery and treatment efficacy**  
The tumor-targeting delivery was investigated by using the DiR dye-labeled liposomes via i.v. injection. The in vivo biodistribution results in the CT26 tumor-bearing Balb/c mice showed that the P-Lipo increased the intratumoral drug distribution and prolonged intratumoral drug retainment compared to the Lipo (Fig. 3a). At the endpoint, the ex vivo imaging of the dissected organs further

confirmed higher intratumoral accumulation in the P-Lipo-treated group (Fig. 3b, c), showing the enhanced tumor distribution via anti-PD-L1-mediated active targeting delivery.

Furthermore, the treatment efficacy of P-Lipo in the subcutaneous CT26 tumor mice was conducted at a dose of 45 mg/kg IRI and 15 mg/kg JQ1. The treatment with single IRI or JQ1 only showed moderate tumor regression, while the comb IRI/JQ1 and the liposomal formulations yielded the synergistic effect. Importantly, the P-Lipo showed the best therapeutic efficacy with a remarkable inhibition of tumor growth and prolonged survival time (Fig. 3d, e). The preliminary safety evaluation showed there were no major pathological changes in the major organs (Fig. S4), suggesting the biocompatibility.

#### Anticancer immunity activated by P-Lipo treatment

CT26 colon cancer is characterized by its microsatellite stability and the consequent less-immunogenic nature [23, 24]. Therefore, the P-Lipo-based chemo-immunotherapy strategy was investigated in the CT26 tumor-bearing mice. The immunohistochemical and immunofluorescence analysis in the tumor clearly showed that the P-Lipo treatment yielded a high level of cleaved caspase 3 (Fig. 4a), which consequently induced irreversible cell apoptosis, and induced the ICD effect as reflected by the CRT expression (Fig. 4b).

It has been recognized that some specific chemotherapeutics can induce ICD effect that triggers antitumor immune responses and thus synergistically work with immunotherapy [25]. To elucidate the anticancer immune responses elicited by the P-Lipo, the immune cells were analyzed. The P-Lipo treatment promoted the maturation of DCs ( $\text{CD11c}^+\text{CD80}^+\text{CD86}^+$ ) in the LN, with a higher maturation percentage than other groups (Fig. 4c).



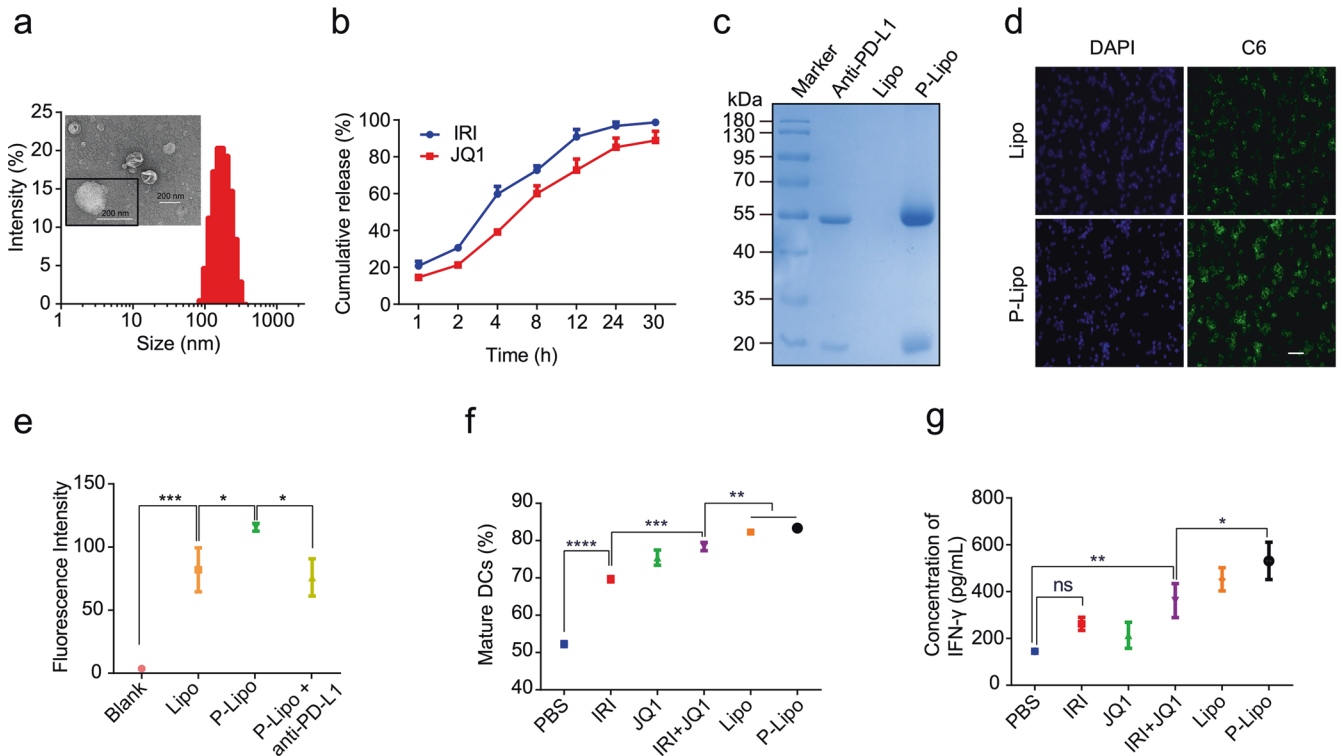


**Fig. 2 Characterization of P-Lipo and immune priming effects.** **a** Size distribution and TEM images of P-Lipo (scale bar 200 nm). **b** Cumulative release of IRI and JQ1 from P-Lipo. **c** SDS-PAGE electrophoresis of anti-PD-L1, Lipo and P-Lipo. **d** Fluorescence images of CT26 cells after incubation with the coumarin 6-labeled liposomes (scale bar 100 μm). **e** Statistical analysis of uptake efficiency of P-Lipo with or without pretreatment with anti-PD-L1 in CT26 cells. **f** Percentage of the mature DCs that were activated by the P-Lipo-treated CT26 cells. **g** IFN-γ secretion from the T cells primed with the mature DCs. Mean ± SEM. \* $P < 0.05$ , \*\* $P < 0.01$ , \*\*\* $P < 0.001$ , and \*\*\*\* $P < 0.0001$

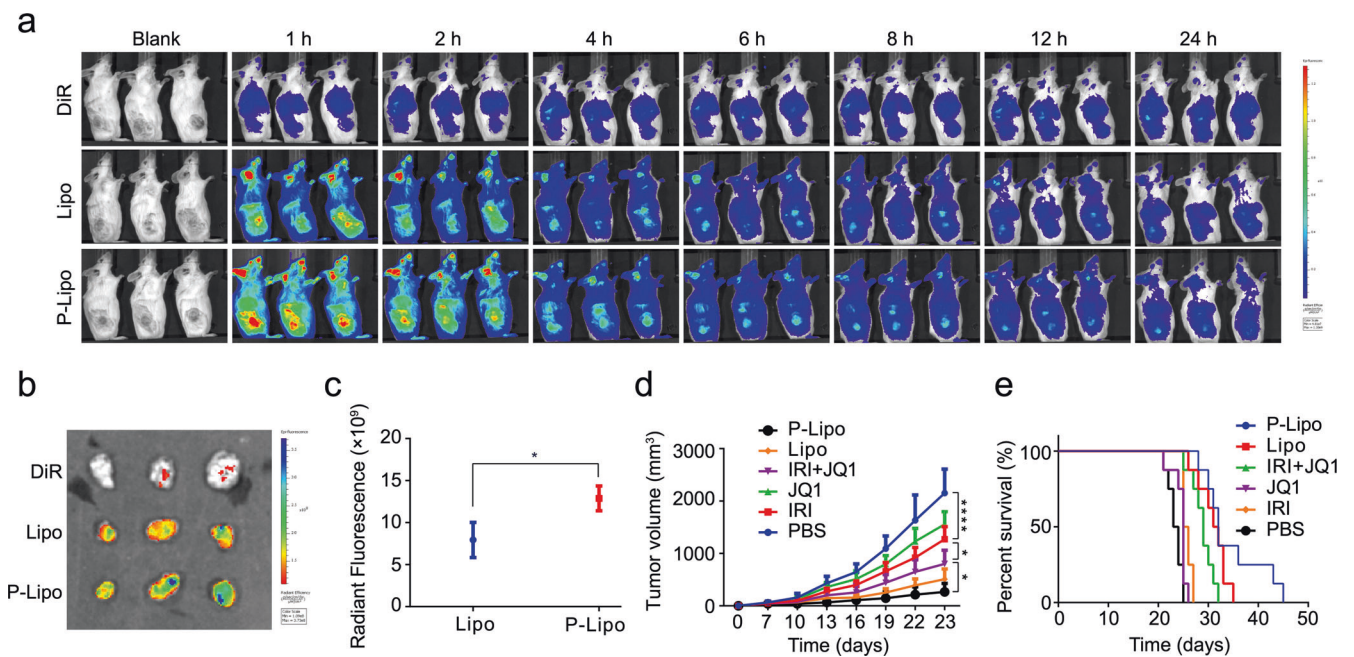


**Fig. 3 Tumor-targeting delivery and in vivo therapy of the P-Lipo.** **a** Whole body imaging. **b** Ex vivo imaging of the tumors. **c** Ex vivo radiant fluorescence in the CT26 tumor-bearing mice following the indicated treatments. **d** The tumor growth curves in the CT26 tumor-bearing mice following the indicated treatments. **e** The survival rate after treatment. Mean ± SEM. \* $P < 0.05$ , \*\*\*\* $P < 0.0001$ .

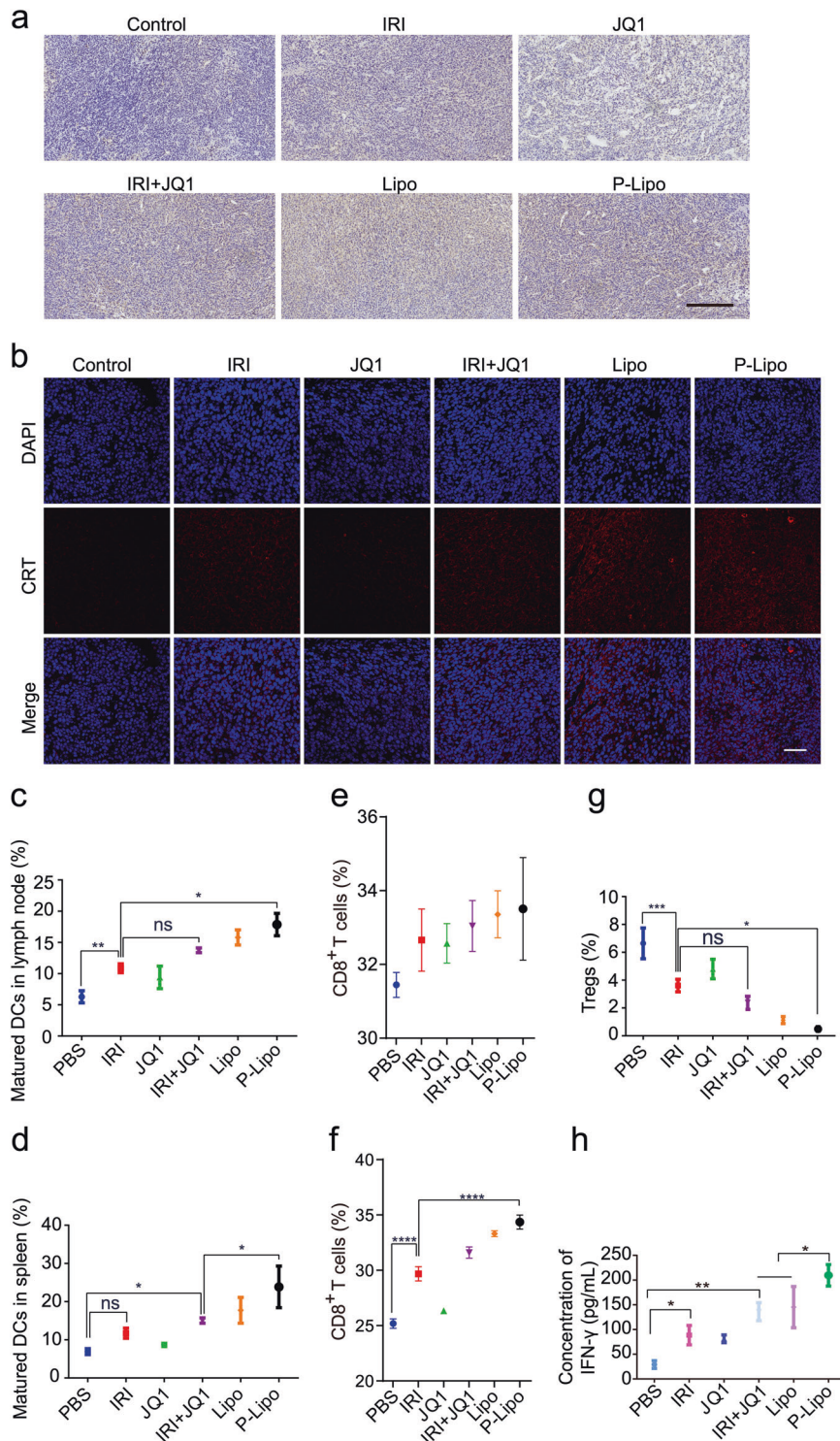


**Fig. 4 P-Lipo-induced anticancer immunity.** **a** Immunohistochemical staining of apoptotic protein (cleaved caspase 3, represented by brown color) (scale bar 250 μm). **b** Immunofluorescence staining of CRT in the tumor (red color) (scale bar 50 μm). **c** Percentage of the mature DCs in the draining LNs. **d** Percentage of the mature DCs in the spleen. **e** CD8<sup>+</sup> T cells in the draining LNs. **f** CD8<sup>+</sup> T cell in the spleen. **g** The frequency of Tregs in the spleen. **h** Serum IFN-γ levels after treatment. Mean ± SEM. \**P* < 0.05, \*\**P* < 0.01, and \*\*\*\**P* < 0.0001.

Moreover, the splenic DCs in the P-Lipo treated mice also showed a higher rate of maturation than other groups (Fig. 4d).

Mature DCs can initiate immune responses by expressing lymphocyte co-stimulatory molecules and presenting antigens [26]. The ratio of CD3<sup>+</sup>CD8<sup>+</sup> cytotoxic T lymphocytes was evaluated. The CD3<sup>+</sup>CD8<sup>+</sup> cytotoxic T lymphocytes in the animals

treated with the P-Lipo were remarkably increased in the LN (Fig. 4e) and spleen (Fig. 4f). The CD4<sup>+</sup>Foxp3<sup>+</sup> Tregs are responsible for immunologic tolerance and reduction of Tregs can provoke cancer immunity [27]. Our results showed that The P-Lipo treatment significantly decreased the amount of Tregs in the spleen, compared to other groups (Fig. 4g).

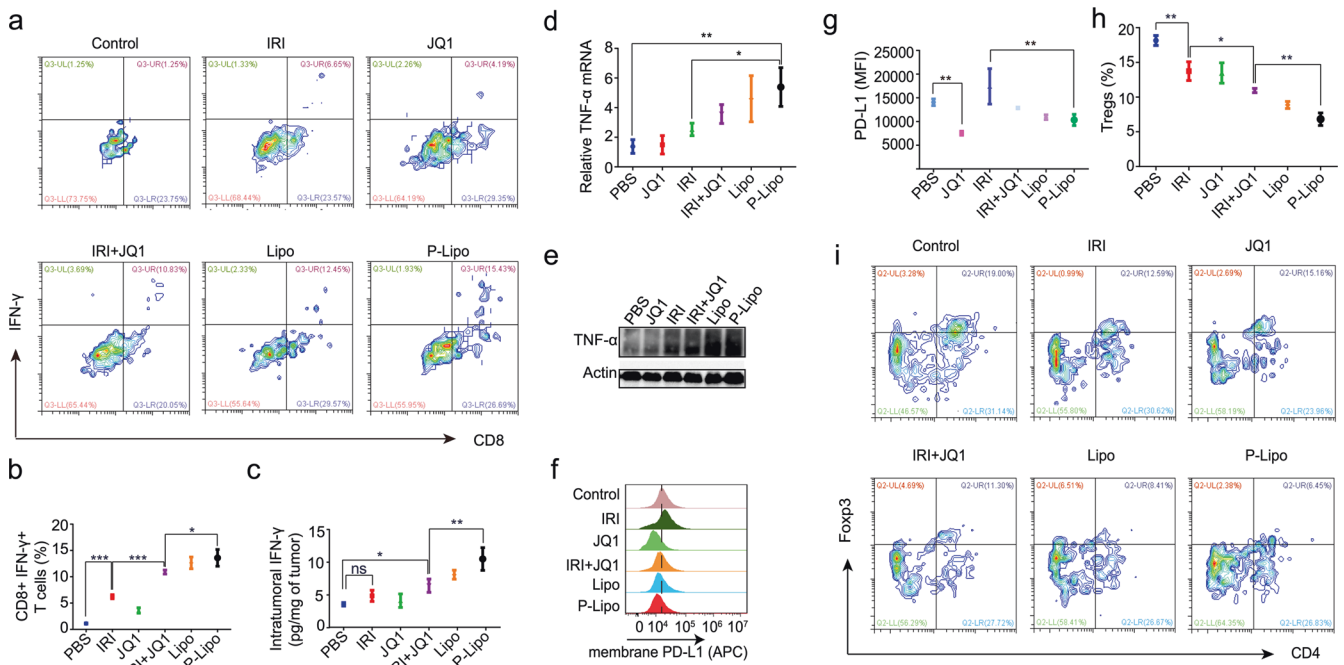


**Fig. 5 Remodeling tumor immune microenvironment.** **a** Flow cytometric scatter-plot of IFN- $\gamma$ <sup>+</sup>CD8<sup>+</sup> T cells in the tumor. **b** The frequency of IFN- $\gamma$ <sup>+</sup>CD8<sup>+</sup> T cells in the tumor. **c** Intratumoral IFN- $\gamma$  levels. The mRNA (**d**) and protein levels of TNF- $\alpha$  (**e**) in the tumor after treatment. **f** Expression of PD-L1 in the tumor cells after treatment. **g** The frequency of PD-L1<sup>+</sup> cells. **h** The frequency of CD4<sup>+</sup>Foxp3<sup>+</sup> Tregs in the tumor. **i** Flow cytometric scatter-plot of CD4<sup>+</sup>Foxp3<sup>+</sup> regulatory T cells in the tumor. Mean  $\pm$  SEM. \* $P$  < 0.05, \*\* $P$  < 0.01, \*\*\* $P$  < 0.001.

IFN- $\gamma$  is an important antitumor effector that controls the initiation, growth, and spread of tumors by mediating pleiotropic effects in the innate and adaptive responses [28]. Serum IFN- $\gamma$  essentially reflects host antitumor immunity and can be a prognostic factor of cancer treatment [29]. The serum IFN- $\gamma$  level in the P-Lipo group was remarkably elevated, with an increase of 2.4-, 1.5-, and 1.4-fold than that of the IRI, IRI-JQ1, and Lipo groups, respectively (Fig. 4h).

These results were consistent with the in vitro results. The superior efficacy of P-Lipo was related to enhanced targeting delivery and the improved synergistic effect of chemo-immunotherapy.

#### Remodeling TIME

IFN- $\gamma$  is mainly produced by activated CD8<sup>+</sup> cytotoxic T cells [30]. Figure 5a, b shows that the percentage of IFN- $\gamma$ -positive cytotoxic CD8<sup>+</sup> T lymphocytes amounted to 13.6% in the tumor in the P-Lipo group, higher than that treated with saline (1.1%), free IRI (6.2%), JQ1 (3.6%), IRI-JQ1 (10.9%), or Lipo (12.6%). Accordingly, the intratumoral IFN- $\gamma$  level in the P-Lipo treatment was also the maximal among all the groups (Fig. 5c). Besides, both the qPCR and Western blotting results showed that the intratumoral TNF- $\alpha$ , a cytokine mainly secreted from the antitumor phenotype macrophages, was highly expressed after the P-Lipo treatment (Fig. 5d, e).

Intratumoral Tregs play an essential role in controlling immunosuppressive TME via regulating cytotoxic T cells, DCs, and macrophages [31]. The ratio of tumor-infiltrating Tregs was decreased to 6.8% in the P-Lipo group compared to 18.2% in the saline control group (Fig. 5h, i). Chemotherapy often induces PD-L1 expression and immunosuppression, which, however, can be overcome through the selection of appropriate drug combinations [32]. Our results showed that the chemotherapeutic IRI upregulated PD-L1 expression in the tumor cells, but the level of PD-L1 was effectively decreased by combination treatment (Fig. 5f, g). It should be mentioned that JQ1 was used to suppress PD-L1 expression, but anti-PD-L1 modified on the P-Lipo was not

designed to block the PD-1/PD-L1 pathway, because the amount of anti-PD-L1 in the P-Lipo given to a mouse was less than 1/10 of the effective therapeutic dose of anti-PD-L1.

These results revealed the remodeling and activation of the TIME by the P-Lipo treatment.

#### CONCLUSIONS

In this work, a chemo-immunotherapy strategy was developed via tumor-targeted codelivery of liposomal IRI and JQ1 for cytotoxicity killing the cancer cells and induced ICD effect that promoted antitumor immune responses and the JQ1-based anti-PD therapy. The P-Lipo showed a synergistic effect on inducing ICD effect and triggering potent antitumor immunity. P-Lipo treatment efficiently inhibited the CT26 tumor growth. It was found that P-Lipo promoted DC maturation and subsequently activated cytotoxic CD8<sup>+</sup> T cells, as well as suppressed Tregs via ICD induction and the PD-pathway blockade. The P-Lipo provides a promising codelivery and chemo-immunotherapy strategy for the less-immunogenic colorectal cancer.

#### ACKNOWLEDGEMENTS

We are thankful for NFSC (81925035, 81673382, and 81521005), and the Strategic Priority Research Program of CAS (XDA12050307), National Special Project for Significant New Drugs Development (2018ZX09711002-010-002), and Shanghai SciTech Innovation Initiative (19431903100, 18430740800) and Shanghai Collaborative Innovation Group of Early Diagnosis and Precise Treatment of Hemangiomas and Vascular Malformations (SSMU-ZDCC20180701) for the support. We thank the Molecular Imaging Center and TEM Facility at SIMM and the National Center for Protein Science Shanghai for technical support.

#### AUTHOR CONTRIBUTIONS

YZH designed the research; ZDH performed the major research; ZDH, MZ, YZH analyzed the data; MZ, YHW, YH, HRW, BFC, BT, and SQZ participated in the cellular and animal studies. ZDH and YZH wrote the paper.



**ADDITIONAL INFORMATION**

The online version of this article (<https://doi.org/10.1038/s41401-020-00570-8>) contains supplementary material, which is available to authorized users.

**Competing interests:** The authors declare no competing interests.

**REFERENCES**

1. Chen L, Han X. Anti-PD-1/PD-L1 therapy of human cancer: past, present, and future. *J Clin Invest*. 2015;125:3384–91.
2. Dermani FK, Samadi P, Rahmani G, Kohlan AK, Najafi R. PD-1/PD-L1 immune checkpoint: potential target for cancer therapy. *J Cell Physiol*. 2019;234:1313–25.
3. Passardi A, Canale M, Valgiusti M, Ulivi P. Immune checkpoints as a target for colorectal cancer treatment. *Int J Mol Sci*. 2017;18:1324.
4. Goldstein J, Tran B, Ensor J, Gibbs P, Wong HL, Wong SF, et al. Multicenter retrospective analysis of metastatic colorectal cancer (CRC) with high-level microsatellite instability (MSI-H). *Ann Oncol*. 2014;25:1032–8.
5. Takamori S, Toyokawa G, Takada K, Shoji F, Okamoto T, Maehara Y. Combination therapy of radiotherapy and anti-PD-1/PD-L1 treatment in non-small-cell lung cancer: a mini-review. *Clin Lung Cancer*. 2018;19:12–6.
6. Mathew M, Enzler T, Shu CA, Rizvi NA. Combining chemotherapy with PD-1 blockade in NSCLC. *Pharmacol Ther*. 2018;186:130–7.
7. Wei J, Long Y, Guo R, Liu X, Tang X, Rao J, et al. Multifunctional polymeric micelle-based chemo-immunotherapy with immune checkpoint blockade for efficient treatment of orthotopic and metastatic breast cancer. *Acta Pharm Sin B*. 2019;9:819–31.
8. Gandhi L, Rodriguez-Abreu D, Gadgeel S, Esteban E, Felip E, De Angelis F, et al. Pembrolizumab plus chemotherapy in metastatic non-small-cell lung cancer. *N Engl J Med*. 2018;378:2078–92.
9. Del Rio M, Mollevi C, Bibeau V, Vie N, Selves J, Emile JF, et al. Molecular subtypes of metastatic colorectal cancer are associated with patient response to irinotecan-based therapies. *Eur J Cancer*. 2017;76:68–75.
10. Haggerty TJ, Dunn IS, Rose LB, Newton EE, Martin S, Riley JL, et al. Topoisomerase inhibitors modulate expression of melanocytic antigens and enhance T cell recognition of tumor cells. *Cancer Immunol Immunother*. 2011;60:133–44.
11. McKenzie JA, Mbofung RM, Malu S, Zhang M, Ashkin E, Devi S, et al. The effect of topoisomerase I inhibitors on the efficacy of T-cell-based cancer immunotherapy. *J Natl Cancer Inst*. 2018;110:777–86.
12. Frey B, Stache C, Rubner Y, Werthmoller N, Schulz K, Sieber R, et al. Combined treatment of human colorectal tumor cell lines with chemotherapeutic agents and ionizing irradiation can in vitro induce tumor cell death forms with immunogenic potential. *J Immunotoxicol*. 2012;9:301–13.
13. Floyd SR, Pacold ME, Huang Q, Clarke SM, Lam FC, Cannell IG, et al. The bromodomain protein Brd4 insulates chromatin from DNA damage signalling. *Nature*. 2013;498:246–50.
14. Wang H, Tang Y, Fang Y, Zhang M, Wang H, He Z, et al. Reprogramming tumor immune microenvironment (TIME) and metabolism via biomimetic targeting codelivery of Shikonin/JQ1. *Nano Lett*. 2019;19:2935–44.
15. Zhu H, Bengsch F, Svoronos N, Rutkowski MR, Bitler BG, Allegranza MJ, et al. BET bromodomain inhibition promotes anti-tumor immunity by suppressing PD-L1 expression. *Cell Rep*. 2016;16:2829–37.
16. Kroemer G, Galluzzi L, Kepp O, Zitvogel L. Immunogenic cell death in cancer therapy. *Annu Rev Immunol*. 2013;31:51–72.
17. Paull TT, Rogakou EP, Yamazaki V, Kirchgessner CU, Gellert M, Bonner WM. A critical role for histone H2AX in recruitment of repair factors to nuclear foci after DNA damage. *Curr Biol*. 2000;10:886–95.
18. Moles E, Urban P, Jimenez-Diaz MB, Viera-Morilla S, Angulo-Barturen I, Busquets MA, et al. Immunoliposome-mediated drug delivery to plasmodium-infected and non-infected red blood cells as a dual therapeutic/prophylactic antimalarial strategy. *J Control Release*. 2015;210:217–29.
19. Carreno BM, Magrini V, Becker-Hapak M, Kaabinejadian S, Hundal J, Petti AA, et al. Cancer immunotherapy. A dendritic cell vaccine increases the breadth and diversity of melanoma neoantigen-specific T cells. *Science*. 2015;348:803–8.
20. Hargadon KM. Strategies to improve the efficacy of dendritic cell-based immunotherapy for melanoma. *Front Immunol*. 2017;8:1594.
21. Banchereau J, Briere F, Caux C, Davoust J, Lebecque S, Liu YJ, et al. Immunobiology of dendritic cells. *Annu Rev Immunol*. 2000;18:767–811.
22. Chen Q, Liu L, Lu Y, Chen X, Zhang Y, Zhou W, et al. Tumor microenvironment-triggered aggregated magnetic nanoparticles for reinforced image-guided immunogenic chemotherapy. *Adv Sci*. 2019;6:1802134.
23. Yu G, Wu Y, Wang W, Xu J, Lv X, Cao X, et al. Low-dose decitabine enhances the effect of PD-1 blockade in colorectal cancer with microsatellite stability by remodeling the tumor microenvironment. *Cell Mol Immunol*. 2019;16:401–9.
24. Chen B, Gao A, Tu B, Wang Y, Yu X, Wang Y, et al. Metabolic modulation via mTOR pathway and anti-angiogenesis remodels tumor microenvironment using PD-L1-targeting codelivery. *Biomaterials*. 2020;255:120187.
25. Maletzki C, Wiegele L, Nassar I, Stenzel J, Junghanss C. Chemo-immunotherapy improves long-term survival in a preclinical model of MMR-D-related cancer. *J Immunother Cancer*. 2019;7:8.
26. Street SE, Cretney E, Smyth MJ. Perforin and interferon-gamma activities independently control tumor initiation, growth, and metastasis. *Blood*. 2001;97:192–7.
27. Sakaguchi S, Sakaguchi N, Shimizu J, Yamazaki S, Sakihama T, Itoh M, et al. Immunologic tolerance maintained by CD25<sup>+</sup>CD4<sup>+</sup> regulatory T cells: their common role in controlling autoimmunity, tumor immunity, and transplantation tolerance. *Immunol Rev*. 2001;182:18–32.
28. Dranoff G. Cytokines in cancer pathogenesis and cancer therapy. *Nat Rev Cancer*. 2004;4:11–22.
29. Lee IC, Huang YH, Chau GY, Huo TI, Su CW, Wu JC, et al. Serum interferon gamma level predicts recurrence in hepatocellular carcinoma patients after curative treatments. *Int J Cancer*. 2013;133:2895–902.
30. Brown TJ, Lioubin MN, Marquardt H. Purification and characterization of cytostatic lymphokines produced by activated human T lymphocytes. Synergistic antiproliferative activity of transforming growth factor beta 1, interferon-gamma, and oncostatin M for human melanoma cells. *J Immunol*. 1987;139:2977–83.
31. Tanaka A, Sakaguchi S. Regulatory T cells in cancer immunotherapy. *Cell Res*. 2017;27:109–18.
32. Gilad Y, Eliaz Y, Yu Y, Han SJ, O'Malley BW, Lonard DM. Drug-induced PD-L1 expression and cell stress response in breast cancer cells can be balanced by drug combination. *Sci Rep*. 2019;9:15099.